PHYSICAL REVIEW E **89**, 050302(R) (2014)

Shear viscosity and structural scalings in model adhesive hard-sphere gels

Aaron P. R. Eberle,[1,2] Nicos Martys,[3] Lionel Porcar,[4] Steven R. Kline,[1] William L. George,[5] Jung M. Kim,[2] Paul D. Butler,[1] and Norman J. Wagner[2]

[1]*NIST Center for Neutron Research, Gaithersburg, Maryland 20899, USA*

[2]*Center for Neutron Science and Department of Chemical & Biomolecular Engineering, University of Delaware, Newark, Delaware 19716, USA*

[3]*Building and Fire Research Laboratory, NIST, Gaithersburg, Maryland 20899, USA*

[4]*Large Scale Structures Group, Institut Laue-Langevin, Grenoble, France*

[5]*NIST Information Technology Laboratory, Gaithersburg, Maryland 20899, USA*

(Received 28 November 2012; revised manuscript received 14 January 2014; published 12 May 2014)

We present experiments and simulations that show a fundamental scaling for both the rheology and microstructure of flowing gels. Unique flow-SANS measurements demonstrate that the structure orients along both the neutral and compression axis. We quantify the anisotropy using a single parameter, α_n, that scales by a dimensionless number, M', that arises from a force balance on a particle. Simulations support the scalings and confirm the results are independent of the shape and range of the potential suggesting a universal for colloidal gels with short-ranged attractions.

DOI: 10.1103/PhysRevE.89.050302 PACS number(s): 83.80.Hj, 47.57.J−, 61.46.Df

Colloidal suspensions are ubiquitous in both nature and industrial materials and have bulk properties that are determined by the delicate interplay between interparticle and external forces and thermal fluctuations [1]. Emergent trends in materials design manipulate interactions to produce systems with specific functionality or predefined properties (a case with infinite technological potential) [2]. While our understanding of the static behavior of colloidal suspensions is becoming clearer, much less is known about how flow influences structure, which is necessary for understanding rheological modeling and processing of gel-based materials [3].

Below the yield stress, gels exhibit many mechanical properties similar to that of an elastic solid. At higher stresses the system flows and a new balance of forces that includes hydrodynamic interactions defines the state of the system leading to structural reorganization over a broad range in length scales. Examples are densification [4,5], fluidization [6], vorticity-aligned roller structures in the bulk [7,8] and under confinement [9], shear-induced displacement of the critical point [10], and structural anisotropy [5,8,11–13] to name a few. The state of the literature on this subject has been reviewed [3]. In particular, rheological measurements provide insight as to how the bulk properties can be scaled by the forces acting on a colloidal particle [14–16]. Flow small-angle neutron scattering (flow-SANS) [11] and small-angle light-scattering [12] measurements reported in the literature have qualitatively identified shear-induced microstructural anisotropy in the form of "butterfly" scattering patterns. The majority of the measurements have been restricted to the velocity-vorticity plane and ultimately an incomplete view of how gels rearrange in the plane of flow (velocity gradient). Furthermore, to date there is no comprehensive experiment or theory that connects flow and the single-particle properties to the dispersion morphology.

In this work we present a quantitative analysis of rheology and scattering experiments complemented by simulations for the adhesive hard-sphere (AHS) model system, which reveals a fundamental scaling behavior for both the microstructure and rheology. The AHS system is of fundamental importance as the first and simplest system that combines hard-sphere excluded volume with interparticle attraction and is a reference system for understanding dispersions with more complex interactions [17]. Rheological and flow-SANS [18] measurements were performed on the AHS dispersions for temperatures below the critical temperature for gelation. We find that under simple shear flow the colloidal microstructure orients along both the neutral direction and compression axis of flow. This microstructural anisotropy is characterized by an order parameter, α_n, that scales with a dimensionless number, M', that arises from a force balance between the flow forces and interparticle attractions. Dissipative particle dynamic (DPD) simulations support the measurements and confirm that the results are indeed independent of the shape of the potential, suggesting that the measurements are universal to colloidal gels with interactions similar to the AHS.

For experiments we use the model octadecyl silica (radius $a = 15$ nm and polydispersity PD $= 0.10$) suspended in n-tetradecane. Details of the particle synthesis and purification can be found elsewhere [19,20]. For this system $\Phi(r)$ is temperature dependent and is a direct manifestation of a fluid-to-solid phase transition of the surface brush layer [19]. This is in contrast to depletion gels in which aggregation is driven by entropy and manifests in experiments as an effective attraction. Previously we characterized the fluid-to-solid phase transition in direct relation to the $\Phi(r)$ over a wide concentration range of $0.09 \leqslant \phi \leqslant 0.52$ using a combination of rheology, fiber-optic quasielastic light scattering, and SANS [20,21].

The steady shear rheology displays a strong temperature dependence, which has also been studied by others [14,15]. This can be seen in Fig. 1(a) for one dispersion of concentration $\phi = 0.21$ and temperatures relative to the critical temperature for gelation $T^* = 29.4 \pm 0.1\,^{\circ}\mathrm{C}$, $\Delta T = (T^* - T)$ [22]. For $T \gg T^*$ ($T > \sim 32\,^{\circ}\mathrm{C}$) the viscosity is Newtonian for all concentrations and shear rates tested. In this regime attractions are negligible and the accessible Péclet number, $\mathrm{Pe} = 6\pi\dot{\gamma}\mu_s a^3/k_B T$ (where $\dot{\gamma}$ is the shear rate, μ_s is the Newtonian solvent viscosity, and k_B is Boltzmann's constant) is within the range of $\mathrm{Pe} \ll 1$ where no structural

 ©2014 American Physical Society

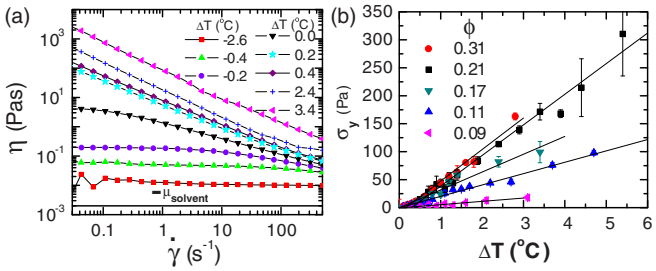

FIG. 1. (Color online) (a) The steady shear viscosity as a function of temperature relative to the critical temperature of gelation, $\Delta T = (T^* - T)$, and shear rate, $\dot{\gamma}$, for a dispersion of concentration $\phi = 0.21$. (b) The yield stress σ_y for all concentrations measured.

anisotropy is expected. For Pe $>$ 1 hydrodynamic interactions can lead to structural anisotropy for hard spheres, especially in concentrated dispersions, which can result in nonlinear rheological phenomena such as shear thinning and thickening [23]. As the system is quenched, interparticle attractions lead to particle aggregation and ultimately a strong $\dot{\gamma}$ dependence of the viscosity, $\eta(\dot{\gamma})$. For $T < T^*$ the viscosity displays shear thinning behavior over all shear rates. The measured yield stress, σ_y, can be found in Fig. 1(b). No measurable σ_y was found at temperatures above T^*, but for $T^* > T$ (± 0.1 °C) σ_y is linear with temperature.

SANS measurements were performed for the first time using both a horizontal (1–2 plane) and vertical (1–3 plane) Couette shear cell defined in Fig. 2 [22]. An anisotropic two-dimensional (2D) scattering pattern, indicating shear-induced microstructural anisotropy, is observed for the dispersions at temperatures below T^*. Figures 2(a) and 2(b) displays the scattering pattern in the 1–3 plane and 1–2 plane, respectively, for one dispersion concentration $\phi = 0.21$ and for similar potential strength and flow conditions. The "butterfly" lobes lie parallel to the flow direction for the 1–3 plane in agreement with prior observations [5,11,12]. Because of the inverse proportionality between Q space and the characteristic length in real space for a given Q, i.e., $Q \propto L^-1$, this butterfly pattern indicates a microstructure that lies oriented along the neutral direction. The measurements in the 1–2 plane reveals, for the first time, that the butterfly lobes lie parallel to the extensional axis such that the structure is oriented along the compression axis of flow (defined in Fig. 2, bottom left) for length scales of similar dimension to the particle diameter. The 2D intensity in Figs. 2(a) and 2(b) are quantified by the one-dimensional sector average scattering intensities displayed in Figs. 2(c) and 2(d). These measurements clearly show a preferred structural alignment that extends from a few particle diameters in both the neutral and compression axis of flow that is observed for all dispersions measured in the parameter space where structural anisotropy was observed. Similar anisotropic microstructure has been reported on thermoreversible gels using small angle light scattering, which measures much larger length scales [5]. Various geometric arguments can lead to the scattering observed in both planes. This includes roller structures idealized as rods with their long axis aligned in parallel to the neutral direction and mean center of mass normal along the compression axis or sheets with a similar axial orientation.

For all dispersions the one-dimensional scattering intensity evolves systematically with decreasing temperature at low-Q ($Q < \sim 0.02$ Å^{-1}) from that characteristic of a hard-sphere-like fluid to self-similar fractal-like clusters. An example can be seen in Fig. 3 for one dispersion concentration $\phi = 0.21$ in the fluid state ($T = 40$ °C) and just below T^*. The intensity is dominated by the spatial correlation of particles or structure factor S(Q) for $Q < 0.02$ Å $^{-1}$. The Q range corresponds

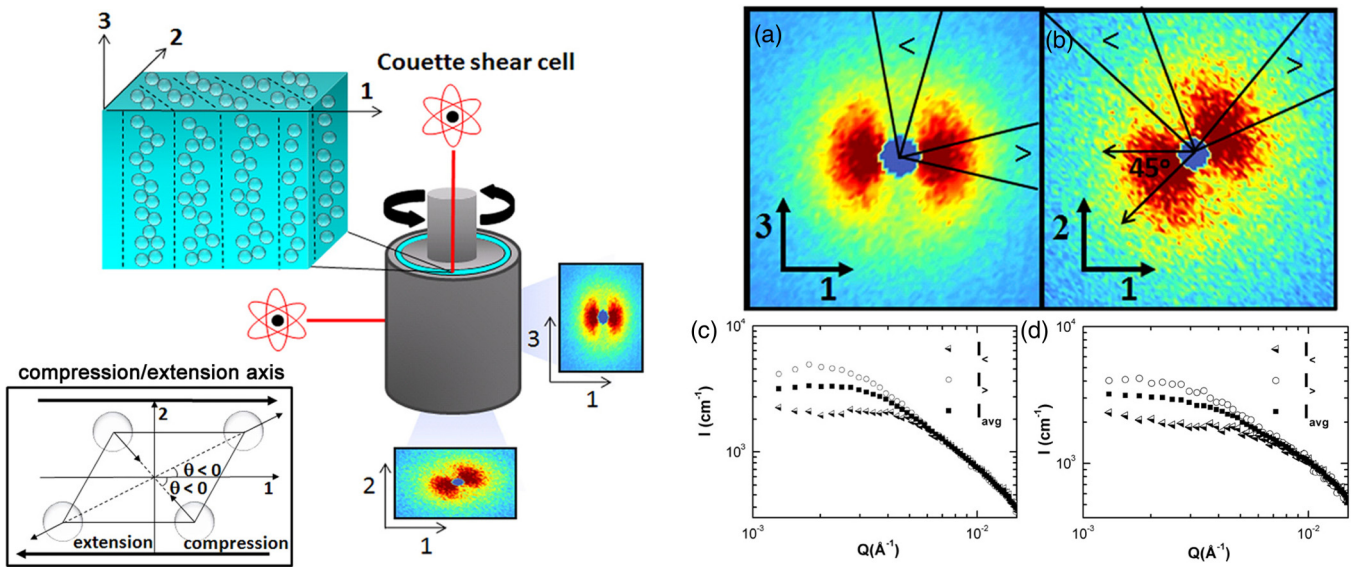

FIG. 2. (Color online) Left side displays the Couette shear cell geometries for horizontal and vertical configurations. A schematic of the sample unit volume suggests the idealized real-space structure. Bottom left defines the axes of compression and extension. Right side: (a) and (b) are the 2D scattering patterns measured in the 1–3 plane and 1–2 plane, respectively. $>$ and $<$ represent the regions over which the sector average scattering intensity is plotted in (c) and (d). (c) and (d) depict the sector averaged intensity $I_<$ and $I_>$ defined in the images above and the circular averaged intensity I_{avg}. For all figures (a) to (d) $\phi = 0.21$, and the measurement was performed at $\Delta T = 1.4$ °C and $\dot{\gamma} = 237$ s^{-1}.

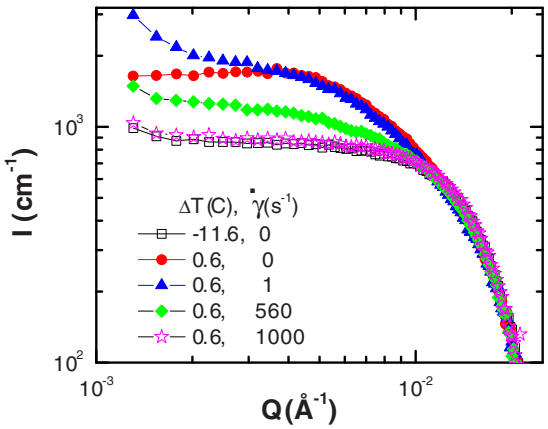

FIG. 3. (Color online) Selected SANS scattering intensity I versus momentum transfer vector Q as a function of temperature, T, and $\dot{\gamma}$, for dispersion concentration $\phi = 0.21$.

to real space structures from the nearest neighbor to ~20 particle diameters in extent. The scattering at $Q >\sim 0.02$ Å^{-1} is largely temperature-independent and reflects the isotropic primary particle characteristics. Shear flow introduces significant hydrodynamic forces causing structural reorganization that follows the general mechanism of cluster densification followed by fluidization with increasing shear. At $\dot{\gamma} = 1.0$ s^{-1} the low-Q scattering intensity increases consistent with densification of the local fractal structure [5,12]. For higher shear rates the scattering intensity continues to evolve with increasing intensity at higher Q followed by a decrease (for all $Q < 0.01$ Å^{-1}). The latter is a direct consequence of shear flow breaking up the fractal clusters. At the highest shear rate tested $\dot{\gamma} = 1000$ s^{-1} the scattering intensity is similar to that observed at rest for high temperatures corresponding to complete fluidization of the local structure. As expected, these corresponding structural states have similar bulk viscosities as seen in Fig. 1(a). Structural fluidization is attributed only to shear forces as the temperature of the sample was directly monitored through the duration of the measurement and viscous heating of the sample was negligible.

We quantify the degree of anisotropy in the system through an order parameter that is calculated by integrating the static subtracted scattering intensity, $\Delta I(Q,\theta) = I(Q,\theta,\dot{\gamma}) - I(Q,\theta,\dot{\gamma} = 0)$, weighted for twofold symmetry, over the azimuthal angle as displayed in Fig. 2 [24]:

$$\Delta H_I(Q) = \frac{1}{2\pi}\int_{\theta_i}^{\theta_i+2\pi} \Delta I\,(Q,\theta)\cos\,(2\theta)\,d\theta. \qquad (1)$$

The angle, θ_i, is defined by a maximum in the intensity. ΔH_I quantifies the Q-dependent changes in the scattering intensity. An equivalent approach has been successfully applied for analysis of the pair distribution function $g(r)$ [25,26]. A unique single parameter quantification of the anisotropy can be defined by integrating ΔH_I over all Q,

$$\alpha = \frac{1}{Q_{\max} - Q_{\min}}\int_{Q_{\min}}^{Q_{\max}} \Delta H_I\,dQ \qquad (2)$$

and normalized by the maximum $\alpha_n = \alpha/\alpha_{\max}$. $Q_{\max}$ is defined by the length scale associated with the particle diameter, $Q \sim 0.02$ Å^{-1}. For this work $Q_{\min}$ was defined by the minimum accessible Q. α_n is bound between 0 and 1 representing an isotropic structure and the greatest degree of anisotropy relative to the static structure, respectively.

For the colloidal gels considered in this work we propose that $\alpha_{\rm n}$ scales by a dimensionless quantity, M', defined as the force due to flow normalized by the maximum interparticle force [27],

$$M' \equiv \frac{6\pi\mu_s a^2\dot{\gamma}}{F_{\max}}, \qquad (3)$$

where μ_s and $F_{\max}$ are the solvent viscosity and maximum interparticle force. By definition $F_{\max}$ is the maximum slope of the pair potential $F_{\max} = (d\Phi/dr)_{\max}$ and can only be directly determined with knowledge of the shape of the potential. An experimentally accessible quantity is σ_y, which is directly proportional to $F_{\max}$ by the relation $\sigma_y \sim \phi^2/a^2(d\Phi/dr)_{\max}$ [28]. With substitution, $M' = C\mu_s\dot{\gamma}\phi^2/\sigma_y$ (where C is a constant) and is independent of particle size. Written in this form M' is similar to the reciprocal of the dimensionless Bingham number. Complementary DPD simulations were performed on dispersions with specified interactions to determine C by mapping the experimental viscosity onto the simulated viscosity [22]. We find $C = 10 \pm 3$ for all concentrations and temperatures measured.

The steady shear viscosity flow curves for all the samples measured are displayed in Fig. 4(a) and compared against the simulations. For both the experiments and simulations we find the viscosity scales by M' and is independent of the shape of the potential for short-ranged attractive systems. As $M' \to 1$ the shear forces become comparable to the force of attraction between individual particles in the gel and are where the viscosity tends toward the high shear rate limiting viscosity. The degree of flow-induced anisotropy shows strong nonmonotonic dependence on shear rate that further depends on temperature and concentration. Remarkably, the microstructural distortion is also found to scale by M'. This result is plotted in Fig. 4(b) for all concentrations measured $0.9 < \phi < 0.21$ and temperature (interparticle potential) bound by the dynamical arrest transition and the gas-liquid coexistence region of the phase diagram and includes both measurements of the 1–3 plane and the 1–2 plane. For all the varied experiments $\alpha_{\rm n}$ collapses onto a single curve with maximum $\alpha_{\rm n} \sim 0.005$. For $M' \ll 0.005$ interparticle forces dominate and maintain the structural integrity within clusters formed as the system yields to flow. For M' around 0.005 flow stretches these clusters along the extension flow axis and forces them together along the compression axis (leading to densification) and resulting in butterfly scattering in both scattering planes. For $M' > 0.005$ the shear forces acting on the clusters are sufficient to reduce their overall size leading to a decay in $\alpha_{\rm n}$. Eventually, the force acting to break up the structure becomes comparable to the interparticle force, and the system is able to fully fluidize into dispersed primary particles at $M' \sim 1$ causing $\alpha_{\rm n} \to 0$ and $\eta(\dot{\gamma}) \to \eta_\infty$. This is seen in Fig. 3 for the highest shear rates, where the angle-averaged scattering intensity corresponds to that of the primary colloids rather than aggregates.

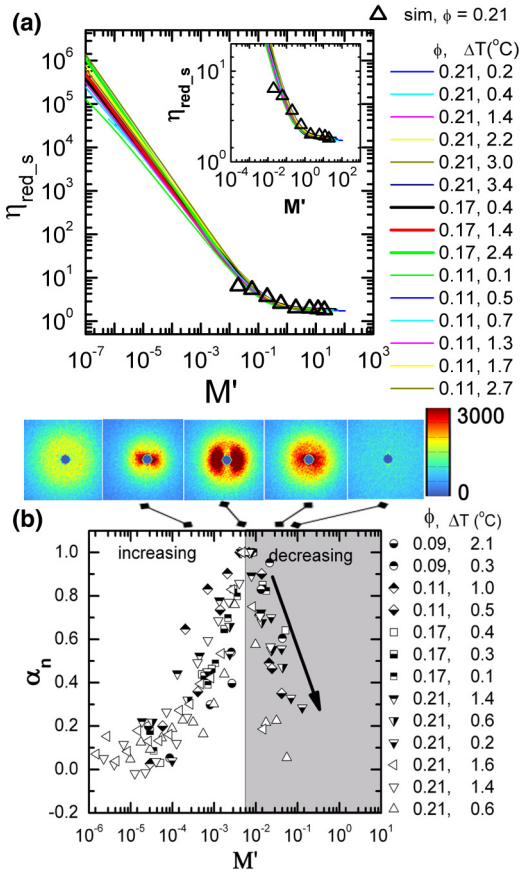

FIG. 4. (Color online) (a) Reduced steady shear viscosity, $\eta_{red} = \eta(\dot{\gamma})/\mu_s$ where μ_s is the solvent viscosity. Solid lines are Carreau-Yasuda fits to experimental viscosity, and open triangles are the DPD simulations for a fixed concentration $\phi = 0.21$ and three different potentials [22]. Error bars represent estimated percent error of the DPD simulation. (b) Normalized anisotropy parameter α_n, scaled by M'. Open symbols represent scattering experiments in the 1–3 plane, and partially filled symbols were performed along the 1–2 plane. 2D scattering patterns are from a dispersion of $\phi = 0.21$.

The features in Fig. 4(b) in relation to the magnitude of M' are a consequence of deriving M' from a force balance on a particle pair such that the flow force in Eq. (3) scales with the characteristic size of a particle and not a cluster [29]. As the clusters contain a significant number of particles, the flow forces acting to disrupt the attractive bonds between particles will be much larger [30]. A quantitative theory incorporating the shear forces acting on the cluster should be able to predict our empirically observed maximum of the shear-induced anisotropy in the microstructure at $M' \sim 0.005$ by explicitly including the effects of shear on the cluster size.

We have identified a common scaling for both the rheology and the microstructure for a model AHS colloidal gel under flow. In addition, with the aid of simulations we show that this behavior is independent of potential shape and supports the universal behavior of this scaling for colloidal gels with interactions similar to the AHS. Current microstructural kinetics constitutive equations used to model the rheology of particulate suspensions connect the flow to the rate of build-up and breakdown of structure but do not account for structural anisotropy. This is the first quantitative experimental work that connects the shear-induced microstructural anisotropy to the particle properties and flow strength for the AHS model system. These results expand the potential for the development of a predictive constitutive theory.

The authors thank Yun Liu, Robert Leheny, and Jan Mewis for discussion. The funding for A.E. was provided by the National Academy of Science through a NRC postdoctoral fellowship. We acknowledge support from the NSF (DMR-0944772), and the Institut Laue-Langevin for access to SANS instruments. This manuscript was prepared in part under cooperative agreement 70NANB10H256 from NIST, US Department of Commerce. The statements, findings, conclusions, and recommendations are those of the authors and do not necessarily reflect the view of NIST or the US Department of Commerce. The identification of any commercial product or trade name within this paper does not imply recommendation or endorsement by the National Institute of Standards and Technology, nor does it imply that the materials or equipment identified are necessarily the bests available for the purpose.

[1] E. Zaccarelli, J. Phys.: Condens. Matter **19**, 323101 (2007).
[2] V. J. Anderson and H. N. W. Lekkerkerker, Nature (London) **416**, 811 (2002).
[3] J. Vermant and M. J. Solomon, J. Phys.: Condens. Matter **17**, R187 (2005).
[4] C. J. Rueb and C. F. Zukoski, J. Rheol. **41**, 197 (1997).
[5] H. Hoekstra *et al.*, Langmuir **21**, 11017 (2005).
[6] H. Verduin, B. J. de Gans, and J. K. G. Dhont, Langmuir **12**, 2947 (1996).
[7] A. Montesi, A. A. Pena, and M. Pasquali, Phys. Rev. Lett. **92**, 058303 (2004).
[8] J. V. DeGroot *et al.*, J. Colloid Interface Sci. **166**, 404 (1994).
[9] X. Cheng *et al.*, Proc. Natl. Acad. Sci. USA **109**, 63 (2011).
[10] M. P. Lettinga, H. Wang, and J. K. G. Dhont, Phys. Rev. E **70**, 061405 (2004).
[11] A. Woutersen, R. P. May, and C. G. De Kruif, J. Rheol. **37**, 71 (1993).
[12] P. Varadan and M. J. Solomon, Langmuir **17**, 2918 (2001).
[13] H. Hoekstra *et al.*, Langmuir **19**, 9134 (2003).
[14] A. Woutersen and C. G. De Kruif, J. Chem. Phys. **94**, 5739 (1991).
[15] C. J. Rueb and C. F. Zukoski, J. Rheol. **42**, 1451 (1998).
[16] R. de Rooij *et al.*, J. Chem. Phys. **11**, 9213 (1993).
[17] R. J. Baxter, J. Chem. Phys. **49**, 2770 (1968).
[18] A. P. R. Eberle and L. Porcar, Curr. Opin. Colloid Interface Sci. **17**, 33 (2012).
[19] A. P. R. Eberle *et al.*, Langmuir **26**, 3003 (2010).
[20] A. P. R. Eberle *et al.*, Langmuir **28**, 1866 (2012).
[21] A. P. R. Eberle, N. J. Wagner, and R. Castañeda-Priego, Phys. Rev. Lett. **106**, 105704 (2011).

[22] See Supplemental Material at http://link.aps.org/supplemental/10.1103/PhysRevE.89.050302 for rheology methods, SANS methods, DPD methods, Carreau-Yasuda fit of rheology, simulation potentials, and rheology mapping to simulations.
[23] N. J. Wagner and J. F. Brady, Phys. Today **62**, 27 (2009).
[24] B. J. Maranzano and N. J. Wagner, J. Chem. Phys. **117**, 10291 (2002).
[25] N. Koumakis *et al.*, Phys. Rev. Lett. **108**, 098303 (2012).
[26] J. Zausch and J. Horbach, Europhys. Lett. **88**, 60001 (2009).
[27] N. S. Martys *et al.*, Eur. Phys. J. E **35**, 20 (2012).
[28] J. Mewis and N. J. Wagner, *Colloidal Suspension Rheology* (Cambridge University Press, New York, 2012).
[29] R. C. Sonntag and W. B. Russel, J. Colloid. Interface Sci. **113**, 399 (1986).
[30] A. H. Krall and D. A. Weitz, Phys. Rev. Lett. **80**, 778 (1998).